Simulation-Based Unitary Fracking Condition and Multiscale Self-Consistent Fracture Network Formation in Shale

Qinglei Zeng
Applied Mechanics Laboratory,
School of Aerospace Engineering,
Tsinghua University,
Beijing 100084, China

Tao Wang
Applied Mechanics Laboratory,
School of Aerospace Engineering,
Tsinghua University,
Beijing 100084, China

Zhanli Liu
Applied Mechanics Laboratory,
School of Aerospace Engineering,
Tsinghua University,
Beijing 100084, China

Zhuo Zhuang[1]
Applied Mechanics Laboratory,
School of Aerospace Engineering,
Tsinghua University,
Beijing 100084, China
e-mail: zhuangz@tsinghua.edu.cn

*Hydraulic fracturing (fracking) technology in gas or oil shale engineering is highly developed last decades, but the knowledge of the actual fracking process is mostly empirical and makes mechanicians and petroleum engineers wonder: why fracking works? (Bažant et al., 2014, "Why Fracking Works," ASME J. Appl. Mech., **81**(10), p. 101010) Two crucial issues should be considered in order to answer this question, which are fracture propagation condition and multiscale fracture network formation in shale. Multiple clusters of fractures initiate from the horizontal wellbore and several major fractures propagate simultaneously during one fracking stage. The simulation-based unitary fracking condition is proposed in this paper by extended finite element method (XFEM) to drive fracture clusters growing or arresting dominated by inlet fluid flux and stress intensity factors. However, there are millions of smeared fractures in the formation, which compose a multiscale fracture network beyond the computation capacity by XFEM. So, another simulation-based multiscale self-consistent fracture network model is proposed bridging the multiscale smeared fractures. The purpose of this work is to predict pressure on mouth of well or fluid flux in the wellbore based on the required minimum fracture spacing scale, reservoir pressure, and proppant size, as well as other given conditions. Examples are provided to verify the theoretic and numerical models.*
[DOI: 10.1115/1.4036192]

Keywords: unitary fracking condition, multiscale self-consistent fracture network formation, stimulated reservoir volume, shale gas, recovery efficiency prediction

1 Introduction

Shale gas is one of nonconventional natural gases, which exists in shale stratum in the status of adsorption and separation, as well as in fluid state. Shale gas preservation in China is widespread with large reserves and low natural abundance. Most shale beds are continental formations undergoing strong late reformation, more acute fault, and tectonic movement. A large number of fractures and microvoids, as well as bedding, jointing, and interlayers exist in heterogeneous shale stratum. The typical cover depths of the gas bearing shale stratum in Sichuan and Chongqing areas are about 2.3–3.6 km with the thicknesses of about 40 m, as shown in Table 1. The overburden pressure generally exceeds the horizontal tectonic stress. Consequently, most fractures must be essentially vertical and few horizontal fractures can be formed.

Hydraulic fracturing (fracking) technology in gas or oil shale engineering is highly developed last decades in North America and also recent years in China, but the knowledge of the actual fracking process is mostly empirical and makes mechanicians and petroleum engineers wonder: why fracking works? [1]. Only 5–15% oil or gas is exploited based on output prediction [1]. From statistics data of six shale gas fields in U.S., there are about 30% perforation clusters which do not contribute to the production [2,3]. Thus, there is a huge challenge and opportunity for engineering mechanics.

In fracking operation, several clusters of fractures are usually initiated and driven to propagate simultaneously and major fractures are generated from perforation clusters. The simultaneous propagation of all major fractures is the guarantee of sufficient stimulation of the whole reservoir. As for the generation of fracture network, one possibility is due to fracture branching at fracture tips. But, such branching is possible only for dynamic cracks propagating in homogeneous material with a velocity faster than 0.4 times Rayleigh wave speed [4]. Whereas the shale rock is inhomogeneous material and fracking in shale is generally a quasi-static process, except for small crack jumps due to heterogeneities that cause acoustic emissions [5]. Fracture speed, which is dependent on fluid flux, is generally only a few millimeters per

Table 1 Shale gas reservoirs in Sichuan and Chongqing areas of China

Region	Changning	Weiyuan	Jiaoshiba
Area (km^2)	2050	4216	485
Cover depth (m)	2300–3200	2400–3600	2400–3500
Shale thickness (m)	33.4–46	40–50	38–44
Clay content (%)	23.9–32.1	30.4–39	17–35
Brittle mineral content (%)	57.8–60.1	50–62.4	56–83
Porosity (%)	3–5.2	3.0–4.6	2.5–7.1
Total organic carbon (%)	2.8–5.3	2.2–3.3	2.0–6.0
Gas content (m^3/ton)	4.86–5.5	4.3–4.79	4.74–5.69
Pressure coefficient	1.35–2.03	1.4–1.96	1.35–1.55
Reservoir pressure (MPa)	31.6–49.9	35.1–67.3	31.0–38.0
Crustal deformation	Thrust	Strike-slip	Strike-slip

[1]Corresponding author.

Manuscript received December 27, 2016; final manuscript received March 7, 2017; published online March 24, 2017. Editor: Yonggang Huang.

second in a large physical experiment with a size of one cubic meter and a few meters per minute in engineering field. Hence, no V-shaped branching at crack tips is considered here. Another possibility considered in this paper is the interactions between hydraulic fractures (HFs) and natural fractures (NFs), faults and voids, which can fully stimulate the reservoirs and result in millions of smeared fractures to link the fracture network. The recent analysis based on the data from five observations in U.S. in 26 months and a typical permeability of shale draws the conclusion that the fracture spacing should be in an order of 0.1 m [1], which means a smeared fracture network is generated.

The significant achievements of applied mechanics in 20th century are finite element method and fracture mechanics. In 21st century, it is a favorable position for their application in high-efficient production of shale gas or oil. A lot of efforts have been dedicated to the research of hydraulic fractures both analytically and numerically in the literatures. For the analytical models of a single hydraulic fracture propagation, the works in Refs. [6–13] can be referred to. The analysis of multiple HFs propagation can be found in Refs. [2] and [14–19]. In this paper, a fully coupled numerical method based on XFEM is adopted to simulate the propagation of multiple major HFs, which can model arbitrary fracture propagation without element remeshing [20]. However, there are millions of smeared fractures, which are beyond the computation capacity with XFEM. Crack band model with equivalent damage over an element with the size of crack spacing is adopted to model HFs branching in Ref. [5]. In this paper, a multiscale fracture model is established to bridge multiscale fractures in shale. It provides a multiscale self-consistent fracture network model, which can be used to estimate the total influx and evaluate output in field engineering eventually.

This paper is organized as follows. In Sec. 2, a simplified two-dimensional physical model is introduced and the corresponding governing equations are given. The numerical method adopted for modeling fluid and solid coupling problem is also briefly described. In Sec. 3, unitary fracking condition is introduced and the simultaneous propagation of multiple fractures is simulated. Then, the multiscale self-consistent fracture network model is developed in Sec. 4. The conclusions and future works are given in Sec. 5.

2 Theoretical Model for Fluid–Solid Coupling

2.1 Governing Equations for Rock. As shown in Fig. 1, multiple fractures are driven to propagate simultaneously in the shale formation initiating from perforation clusters located on a horizontal wellbore. Plane strain assumption is adopted for the rock formation and the problem is simplified into two dimensions in the horizontal plane, which is also called the KGD model (named after pioneering researchers Kristianovic, Geertsma, and de Klerk) [6,7]. The system is symmetric with respect to an axis of the wellbore and only half of the geometry is depicted and simulated. The fractures usually propagate along the direction of maximum principal tectonic stress σ_H. The minimum principal tectonic stress is σ_h. The total pumping flux Q_0 is partitioned into each major fracture along the wellbore. The radius of wellbore is a and the height of formation is h. Strictly speaking, there should be a transition zone between the wellbore and rock formation with height h, which is neglected in the model.

The solid medium is assumed to be isotropy and no specific bedding layer orientation is considered. It is assumed to be linear-elastic with Young's modulus E and Poisson's ratio ν, as well as impermeable. The body force is neglected and stress $\boldsymbol{\sigma}$ should satisfy the equilibrium equation

$$\nabla \cdot \boldsymbol{\sigma} = 0 \tag{1}$$

The strain $\boldsymbol{\varepsilon}$ can be computed from displacement $\mathbf{u}$ as

$$\boldsymbol{\varepsilon} = \frac{1}{2}\left[\nabla \mathbf{u} + (\nabla \mathbf{u})^{\mathrm{T}}\right] \tag{2}$$

and can be related with $\boldsymbol{\sigma}$ by the constitutive equation

$$\boldsymbol{\sigma} = \mathbf{C} : \boldsymbol{\varepsilon} \tag{3}$$

where $\mathbf{C}$ is an elastic matrix.

The fractures are driven to propagate by the fluid pressure p applied on fracture surfaces and the boundary conditions are written as

$$\boldsymbol{\sigma} \cdot \mathbf{n} = -p\mathbf{n} \quad \text{on} \quad \Gamma_p^+ \quad \text{and} \quad \Gamma_p^- \tag{4}$$

where Γ_p^+ and Γ_p^- are opposite fracture surfaces and $\mathbf{n}$ is an outward unit normal vector of the surface. The displacement boundary and external applied traction boundary should also be satisfied.

The fracturing of shale can be assumed to be brittle and governed by the linear elastic fracture mechanics. If the equivalent stress intensity factor reaches a critical value K_{Ic}, the fracture would propagate [21].

2.2 Governing Equations for Fluid Flow. The fracture opening generates a flow channel for the fluid and the opening width w can be obtained by

$$w = (\mathbf{u}^+ - \mathbf{u}^-) \cdot \mathbf{n}^- \tag{5}$$

where $\mathbf{u}^+$ and $\mathbf{u}^-$ are the displacements on the fracture surfaces Γ_p^+ and Γ_p^-, respectively, and $\mathbf{n}^-$ is the outward normal vector for Γ_p^-. The width is quite a small value compared with the characterized fracture length. The fluid flow is considered to be slow enough to neglect inertial effects as discussed in the Introduction. The effect of proppants on fluid properties and the creep embedment of proppants are neglected. Then, the incompressible fluid flow in the fracture can be approximated as lubrication flow and the governing equation can be expressed as

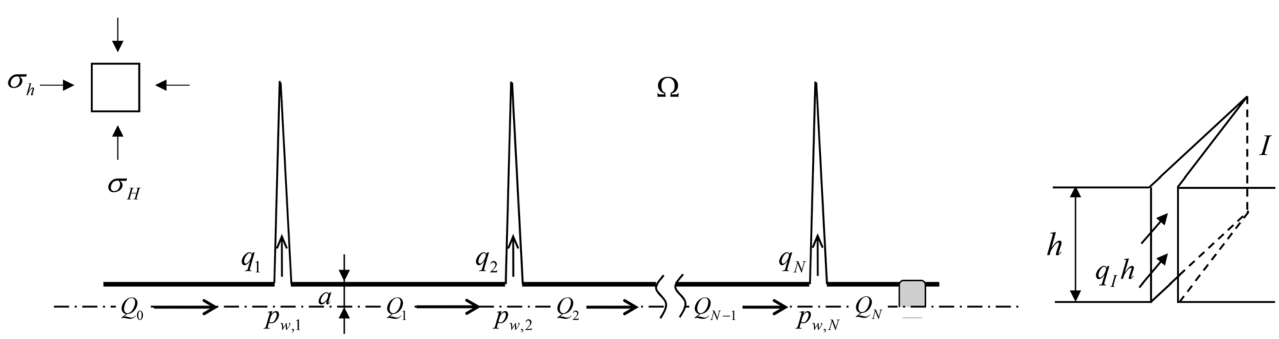

Fig. 1 Simultaneous propagation of multiple fractures during one fracking stage

$$\frac{\partial w}{\partial t} = \frac{\partial}{\partial s}\left(\frac{w^3}{12\mu}\frac{\partial p}{\partial s}\right) \quad (6)$$

where t is time, μ is dynamic viscosity of the fluid, and s is curvilinear coordinate along the fracture with inlet position as the origin. The inlet flow rate of each fracture $q|_{s_I=0}, I = 1, N$ is written as q_I. The boundary conditions at fracture front are given as

$$w_{\text{tip}} = 0, \quad q_{\text{tip}} = 0 \quad (7)$$

where w_{tip} and q_{tip} are the fracture opening width and flow flux at the fracture front, respectively.

As for the fluid flow in a horizontal wellbore, the mass conversation should be satisfied in the following formulations:

$$Q_I = Q_0 - \sum_{J=1}^{I} 2hq_J, \quad I = 1, \ldots, N \quad \text{and} \quad Q_N = 0 \quad (8)$$

The pressure should drop down as the fluid flows along a wellbore because of friction. For a wellbore with length D, the pressure loss Δp_w along the wellbore can be given in Darcy–Weisbach formulation [22]

$$\Delta p_w = g(\text{Re}, e)\frac{D}{2a}\frac{\rho V|V|}{2} \quad (9)$$

in which ρ is the density of fluid, $V = Q/A$ is the cross-sectional averaged fluid velocity, and g is the Darcy friction factor which is a function of the Reynolds number $\text{Re} = 2a\rho|V|/\mu$ and the roughness of wellbore e. For relatively smooth pipes, the influence of roughness can be neglected and g can be approximated as

$$g = \begin{cases} 64/\text{Re}, & \text{for} \quad \text{Re} < 2000 \\ 0.316/\text{Re}^{0.25}, & \text{for} \quad \text{Re} > 4000 \\ 0.0243 + 3.867\text{Re}/10^6, & \text{otherwise} \end{cases} \quad (10)$$

When the fluid flows through a perforation cluster, the local pressure loss can occur because of the perforation entry friction, which is one key effect to promote simultaneous propagation of multiple fractures. This will be revealed in Sec. 3. The local pressure drop can be obtained as [23]

$$p_{w,I} - p_{e,I} = \varphi_{p,I} \cdot 2hq_I \cdot |2hq_I| \quad (11)$$

where $p_{w,I}$ is the pressure in wellbore and $p_{e,I}$ is the pressure at the inlet of fracture I. $\varphi_{p,I}$ is an entry loss coefficient at the entry hole of fracture I. Flow rate q_I is the fluid distribution from wellbore to the ith fracture. φ_p is an empirical coefficient, depending on the number of perforations, hole roughness, perforation diameter, etc.

2.3 Numerical Simulation. Hydraulic fracturing is a fully fluid–solid coupling problem, since the fluid pressure can drive deformation and fracturing of the solid medium and the fractures supply as the flow channels, in turn. The cube of fracture opening width w enters the governing Eq. (6), which results in a nonlinear system. The analytical solution of just one single hydraulic fracture is already complex. It is almost impossible to solve these fully coupled equations for multiple HFs' propagation theoretically. Numerical simulation is described to model the process in this paper. The arbitrary propagation of fractures can be modeled with XFEM and the fluid flow in fractures can be simulated with finite volume method. The displacements of rock $\mathbf{u}$, the pressure along fractures $\mathbf{p}$, and the inlet fluxes of fractures $\mathbf{q}$ are chosen as the basic unknowns. After discretizing the governing equations for rock deformation, fluid flow in fractures, fluid flow in wellbore, and perforation entry loss, we can get a system of nonlinear equations about $(\mathbf{u}, \mathbf{p}, \mathbf{q})$, which is solved by the Newton's iteration. The secant iteration is proposed to determine the new fracture fronts at each time increment. More details on numerical aspects can be found in Ref. [20].

3 Unitary Fracking Condition for Major Fracture Growth

When multiple major fractures are initiated simultaneously, all the fractures are desired to propagate to some distance and the reservoir can be stimulated as much as possible. However, the interaction between different fractures may prevent this ideal propagation topology, and preferential growth of some fractures may occur. On one hand, the stress interaction among the solid medium can induce stress shielding effect [24]. Loss of stability for "dry fracture" system has been studied a lot in the literature [25–28]. On the other hand, the fluid partitioning into different clusters from the wellbore can also affect propagation process, which has been ignored in most of former researches. In this section, a unitary fracking condition is firstly proposed to form a more intuitive understanding of the propagation of HFs, and then, several cases for multiple fractures propagation are studied, which can reveal the process of fluid partitioning and stress intensity factor evolution.

There is a competition mechanism between fluid flux and stress intensity factor to drive the fracture propagation. The inlet flux q for each fracture can be approximated as $q \geq 0$. Even though q is negative at some time, which means the fluid flows out of that fracture, the value is quite small considering the finite fluid volume in a fracture and can be approximated as zero. The fractures are assumed to propagate straightly along the direction of maximum tectonic stress, and the only stress intensity factor K_I for Mode I fracture is considered. The criterion $f = K_I - K_{Ic}$ is always equal to or less than zero corresponding to fracture propagation or arrest, respectively. Thus, conditions $q \geq 0$ and $f \leq 0$ can be combined into a single equation

$$qf = 0 \quad (12)$$

which is called the unitary fracking condition proposed in this paper. There are two cases existing: (1) If $q > 0$, then $f = 0$, which means that the fluid is injected and fracture cluster propagates; (2) if $q = 0$, then $f < 0$, which means that no more fluid is injected and fracture cluster arrests. Numerical results are provided to demonstrate this unitary fracking condition.

The same model is adopted as in Ref. [20]. Four equally spaced fractures with initial lengths 2.1 m are driven simultaneously as shown in Fig. 2 and the parameters are listed in Table 2. Four cases with different conditions are adopted as shown in Table 3. The effects of different critical stress intensity factors, the pressure loss in the horizontal wellbore, and the pressure loss at the perforation entry are investigated. The fluid partitioning and stress intensity factor evolution are extracted and depicted from Figs. 3–6. What should be illustrated is that the evolution of K_I is substituted by $f = K_I - K_{\text{Ic}}$ in these figures, where f is equal to zero when the fracture propagates.

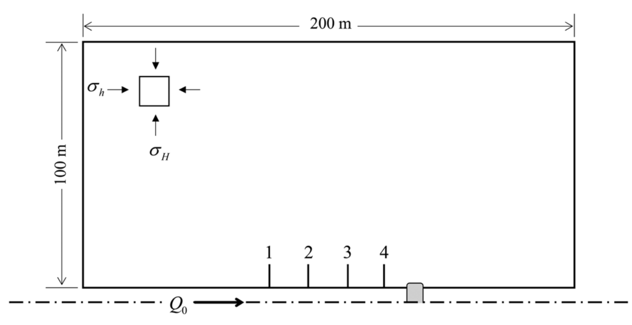

Fig. 2 Simultaneous propagation of four HFs

Table 2 Parameters for simultaneous propagation of four HFs

E	ν	σ_h	σ_H	Q_0	μ	ρ	a	h	D_I
20 GPa	0.2	0 MPa	10 MPa	0.04 m^3/s	0.001 Pa · s	1000 kg/m^3	0.05 m	20 m	10 m

Table 3 Simulation conditions for the cases with four HFs

	K_{Ic}(MPa · $\sqrt{m}$)	Pressure loss in wellbore	Pressure loss at perforation entry
Case 1	3	—	—
Case 2	1	—	—
Case 3	1	√	—
Case 4	1	√	√

Note: "—" means the corresponding effect is neglected and "√" means this effect is included.

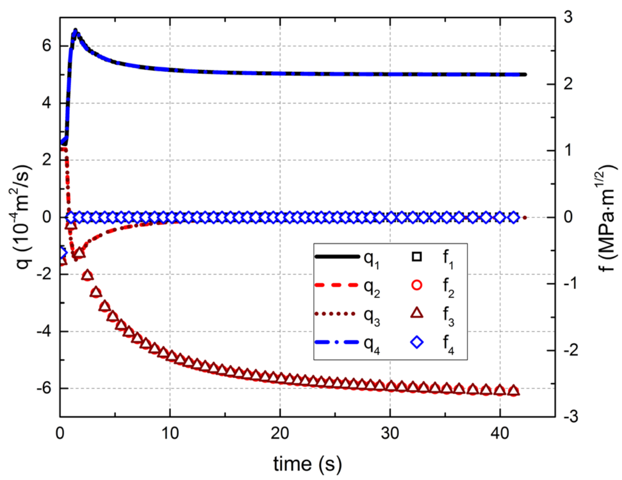

Fig. 3 Fluid partitioning and evolution of *f* for case 1

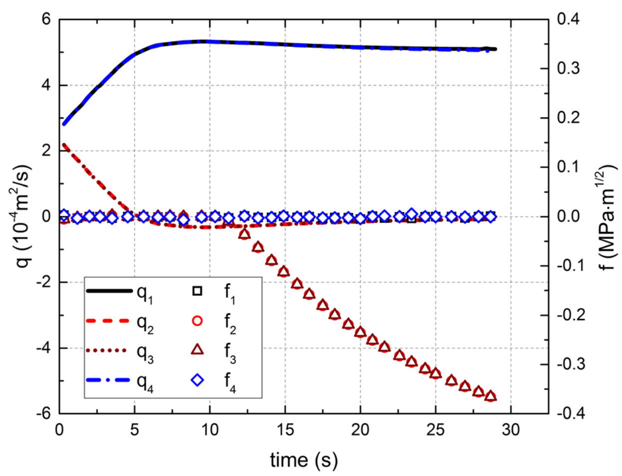

Fig. 4 Fluid partitioning and evolution of *f* for case 2

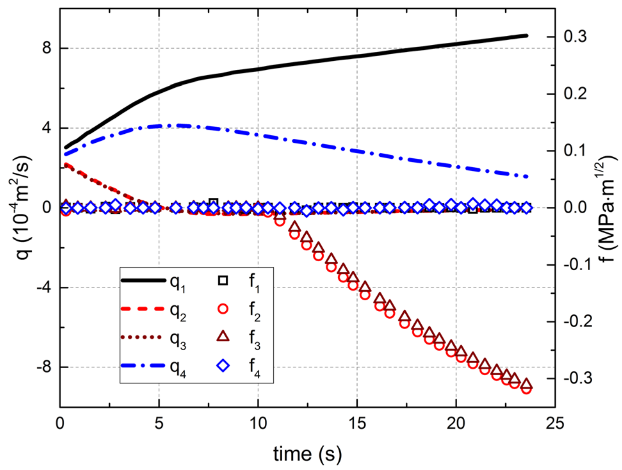

Fig. 5 Fluid partitioning and evolution of *f* for case 3

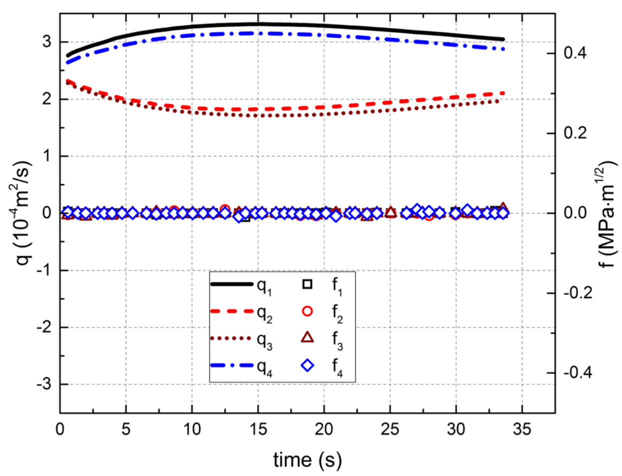

Fig. 6 Fluid partitioning and evolution of *f* for case 4

Case 1 and Case 2: In the two cases, both pressures drop in the wellbore and pressures loss at the perforation entry are neglected. Different toughnesses are considered. The symmetric fractures 1 and 4 are located on the end of left and right sides. The other symmetric fractures 2 and 3 are located closed to the center. The fluid partitioning and evolution of f are also symmetric as shown in Figs. 3 and 4, respectively. The inner fractures are shielded more seriously than the outer fractures and consequently much more fluid flows into fracture 1 and 4, instead of 2 and 3. There are two energy dissipative mechanisms during propagating: the dissipation in viscous flow and dissipation in fracturing rock, which are called viscosity-dominated regime and toughness-dominated regime, respectively. Since initiation, the outer fractures 1 and 4 keep propagating ($f = 0$) and the inner fractures 2 and 3 propagate to some distance and then stop moving. With a smaller toughness, case 2 is more viscosity-dominated than case 1. The inner fractures can propagate longer before stopping in case 2 than in case 1, which is the effect of propagation regime.

Case 2 and Case 3: Compared with case 2, the pressure loss in the horizontal wellbore is included in case 3. If the pressure loss in the wellbore is not considered, the driving pressure in the wellbore is constant and so fracture 1 and 4 can propagate at the same velocity. However, if the pressure loss in the wellbore is included, the pressure will drop along the wellbore and the driving pressure for fracture 1 is larger than that for fracture 4, which results in that more fluid flowing into fracture 1 than fracture 4 as shown in Fig. 5.

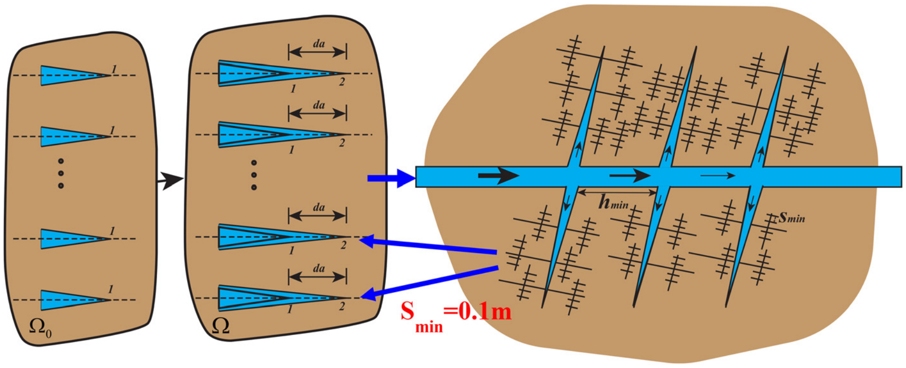

Fig. 7 Global fracture network from local fracture SRV model

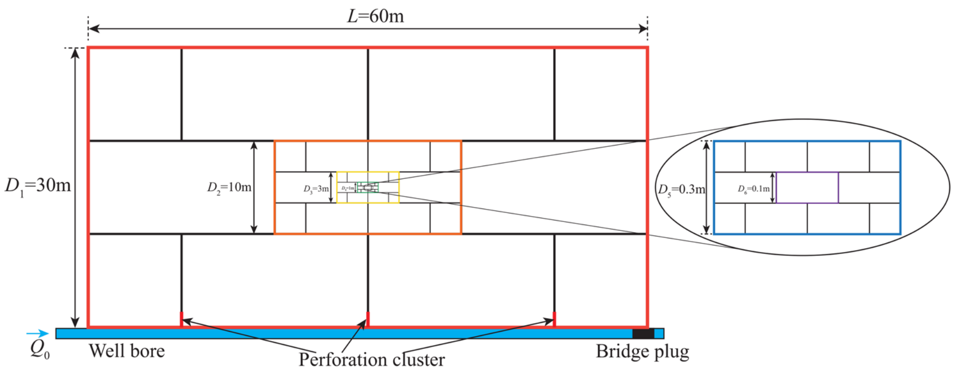

Fig. 8 The smallest fracture spacing 0.1 m is established after five scale reduction from the largest scale level at 30 m

Case 3 and Case 4: In case 4, the perforation entry loss effect is considered, which is called "limited entry technique" in petroleum industry to promote uniform distribution of the fracking fluid into multiple fractures. If more fluid flows into one fracture, more pressure will be lost at the entry of this fracture, which prevents uncontrollable propagation of the fracture. A perforation entry loss coefficient $\varphi_p = 10^3\ \mathrm{MPa} \cdot \mathrm{s}^2/\mathrm{m}^6$ is adopted in case 4. Just as expected, all the fractures can accept a certain amount of fluid and keep propagating as shown in Fig. 6. All four fractures satisfy the criterion with $f = 0$ and unitary fracking condition in Eq. (12).

From the above simulation results of four different cases, it can be concluded that the interactions occurring among both the shale formation (shale toughness) and the flow system (pressure loss in the wellbore and at the perforation entry) can affect the final propagation topology.

4 Multiscale Self-Consistent Fracture Network Model

In Sec. 3, simultaneous initiation and propagation of multiple major fractures from the horizontal wellbore are investigated during one fracking stage. However, there are millions of smeared fractures in the formation, which compose a multiscale fracture network beyond the computation capacity. Thus, another simulation based multiscale self-consistent fracture network model is proposed bridging the multiscale smeared fractures. In the recent analysis, based on the data obtained from five observations in U.S. during 26 months and a typical permeability in nano-Darcy law of shale, the conclusion that the fracture spacing should be in an order of 0.1 m can be drawn [1]. A global fracture network from local fracture stimulated reservoir volume (SRV) model is plotted in Fig. 7, which means a smeared fracture network is generated.

In the actual formation, there are a considerable number of parallel NFs, which may be weak interfaces or joints and they generate an unstimulated fracture network. These NFs are assumed to possess a certain strength. During the propagation of HFs, they may encounter

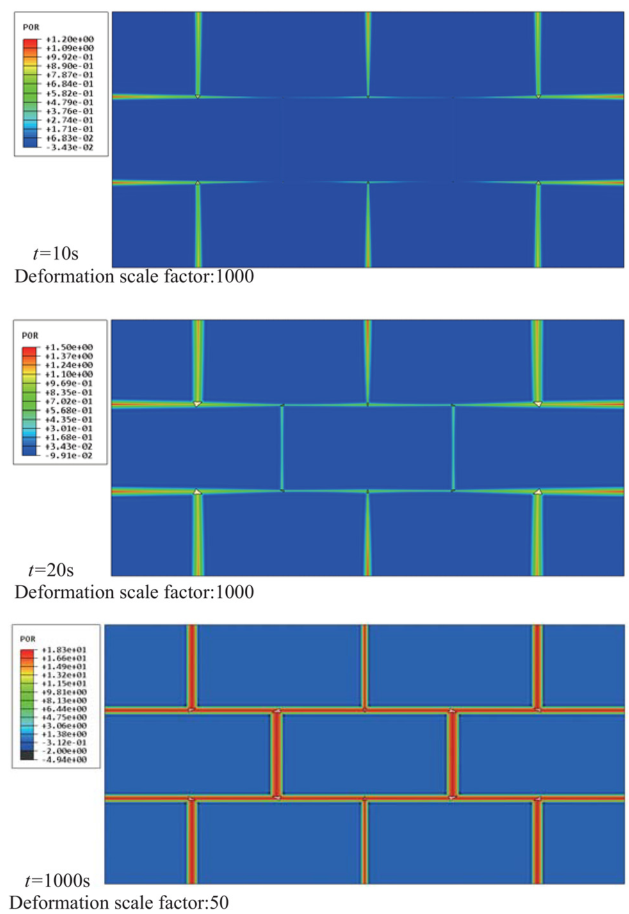

Fig. 9 The fracture propagation process at the smallest scale

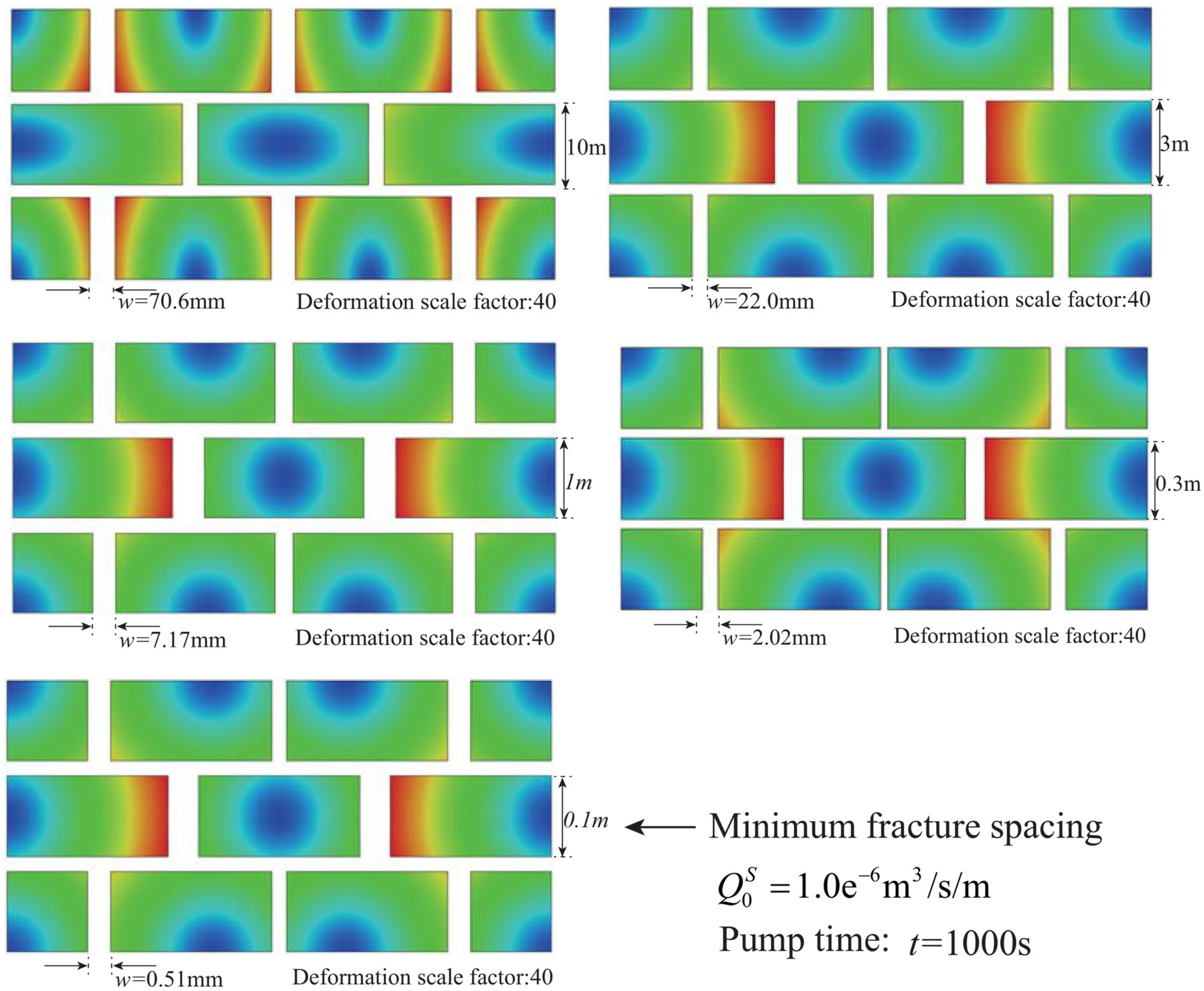

Fig. 10 Fracture width and formation deformation contour at different scales

NFs and reinitiate to the new surfaces of NFs; thus, a brick-type fracture network can be formed as shown in Fig. 8. The nodal force is released or cohesion is debonded along the element edges during fracture propagation and the fracturing criterion is obeyed. If the model is considered from different scales, there will be a similar fracture network at each scale, which can be understood as that the fracture network formed in hydraulic fracturing is multiscale self-consistent structures. The shale gas from minimum scale fracture network gradually flows into the fracture network and ultimately flows into the wellbore. Therefore, the multiscale fracture network model is proposed as shown in Fig. 8. The model with the smallest fracture spacing 0.1 m is established after five scale reduction from the largest scale level at 30 m.

At the smallest scale of fracture network, a fracture can be supported by the proppant and prevented from closing, which is considered as a productive fracture network. Since the size of the common proppant is around 0.5 mm, for example, the diameter of the 40 mesh proppant is 0.425 mm, we define fractures with a width larger than 0.5 mm as the effective fractures. If the width of each fracture in the network exceeds 0.5 mm at the minimum fracture network scale, then the multiscale fracture network is fractured completely. In this case, the injection rate to fracture formation completely can be obtained at the macroscale by deduction from the smallest scale to the largest scale once the fracking treatment time is given.

For the multiscale fracture network model proposed above, the cross-sectional area of the formation is reduced by a factor of 10 for each scale reduction. Therefore, for each scale increase, the injected flow rate is increased by a factor of 10. At the smallest scale (0.1 m fracture spacing), the fracture propagation process is shown in Fig. 9. As the fluid is injected, fractures gradually propagate in the early period of time, and after that, they gradually

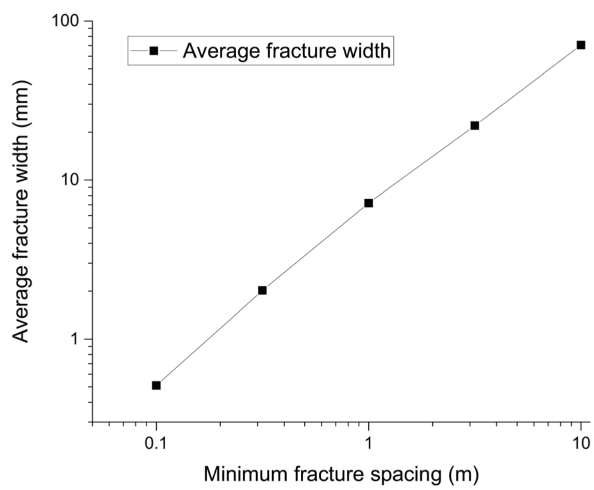

Fig. 11 Average fracture width versus minimum fracture spacing at different scales

Table 4 Significance of fracking to reform fracture network

Input from experiment and field engineering	Cover depth, wellbore length, shale thickness, brittleness, pressure coefficient, reservoir pressure
Field engineering operation	Fluid flow q resulting from minimum fracture spacing and multiscale self-consistent fracture network, perforation friction, cluster distance
Evaluate capacity	Global damage volume ratio to predict recovery efficiency

widen. The NFs have been opened in some regions before the fracking fluid flows into them, because the normal stress in some regions ahead of the propagating fractures may be tensile and opens the NFs, which are viewed as weak interfaces.

At different scales, fracture width and formation deformation contours are shown in Fig. 10. In the smallest scale, if the injection rate of fracturing fluid is $Q_0^S = 1.0 \times 10^{-6}\ \mathrm{m^3/s/m}$ (the unit of flux is such written to emphasize that the thickness of the formation is considered) and the injection time is 1000 s, then the minimum width of fractures can reach 0.5 mm. Scaling up from the smallest scale, the injection rate at the largest scale can be obtained as $Q_0 = 0.01\mathrm{m^3/s/m}$. In other words, for a $60\,\mathrm{m} \times 30\,\mathrm{m} \times 10\,\mathrm{m}$ formation, complete fracturing can be achieved by an injection rate of $Q_0 = 0.01\,\mathrm{m^3/s/m}$ with the injection time as 1000 s. In addition, as can be seen from Fig. 10, the width of the fracture is reduced by approximately three times for each reduction scale.

The average fracture width with respect to the minimum fracture spacing at different scales is shown in Fig. 11. It can be seen that the average fracture width is approximately linear with the spacing scale (with a linear fitting slope $k = 1.06$ in log–log coordinates), which indicates that the fracture network is self-consistent at different length scales.

5 Conclusions

In this paper, the generation of fracture network in fracking is investigated in two levels: the unitary fracture condition for multiple fractures propagation and multiscale self-consistent fracture network model. The uniform partitioning of fluid into multiple fractures is desired in order to stimulate the reservoir as much as possible. The fractures interact with each other because of the stress shielding effect and the fluid flow system. A unitary fracking condition is suggested to feature the propagation of each fracture. In order to generate a fracture network with the minimum spacing, a multiscale self-consistent fracture network is adopted to estimate the total influx.

The final purpose of this work is to predict the pressure on the mouth of the well or the total influx based on the required minimum fracture spacing reservoir pressure and proppant size, as well as other given conditions. The fracking process can be summarized in Table 4. Some parameters can be defined in advance by experiment and field engineering, such as cover depth and wellbore length, shale thickness, brittleness, pressure coefficient, reservoir pressure, and so on. And then, the field engineering operation parameters can be defined and optimized through the aforementioned simulations. Fracking pressure, major fracture distances, and perforation friction loss can be determined by the unitary fracking condition. The fluid pumping rate can be determined by the multiscale self-consistent fracture model. At last, the global damage volume ratio can be adopted to predict recovery efficiency. In order to obtain the damage volume ratio, a damage model for shale should be included to describe the inelastic deformation, which is left for the future work.

Acknowledgment

This work is supported by National Natural Science Foundation of China (Grant Nos. 11532008 and 11372157), the Special Research Grant for Doctor Discipline by Ministry of Education, China (Grant No. 20120002110075), and the Foundation for the Author of National Excellent Doctoral Dissertation of China (Grant No. 201326). Tsinghua University Initiative Scientific Research Program is also acknowledged.

References

[1] Bažant, Z. P., Salviato, M., Chau, V. T., Visnawathan, H., and Zubelewicz, A., 2014, "Why Fracking Works," ASME J. Appl. Mech., **81**(10), p. 101010.
[2] Lecampion, B., and Desroches, J., 2015, "Simultaneous Initiation and Growth of Multiple Radial Hydraulic Fractures From a Horizontal Wellbore," J. Mech. Phys. Solids, **82**, pp. 235–258.
[3] Miller, C. K., Waters, G. A., and Rylander, E. I., 2011, "Evaluation of Production Log Data From Horizontal Wells Drilled in Organic Shales," North American Unconventional Gas Conference and Exhibition, Society of Petroleum Engineers, The Woodlands, Texas, Paper No. SPE-144326-MS.
[4] Xu, D. D., Liu, Z. L., Liu, X. M., Zeng, Q. L., and Zhuang, Z., 2014, "Modeling of Dynamic Crack Branching by Enhanced Extended Finite Element Method," Comput. Mech., **54**(2), pp. 489–502.
[5] Chau, V. T., Bažant, Z. P., and Su, Y., 2016, "Growth Model for Large Branched Three-Dimensional Hydraulic Crack System in Gas or Oil Shale," Philos. Trans. R. Soc. A, **374**(2078), p. 20150418.
[6] Geertsma, J., and De Klerk, F., 1969, "A Rapid Method of Predicting Width and Extent of Hydraulically Induced Fractures," J. Pet. Technol., **21**(12), pp. 1571–1581.
[7] Khristianovic, S. A., and Zheltov, Y. P., 1955, "Formation of Vertical Fractures by Means of Highly Viscous Liquid," 4th World Petroleum Congress, Rome, Italy, June 6–15, Paper No. WPC-6132.
[8] Nordgren, R. P., 1972, "Propagation of a Vertical Hydraulic Fracture," Soc. Pet. Eng. J., **12**(4), pp. 306–314.
[9] Perkins, T. K., and Kern, L. R., 1961, "Widths of Hydraulic Fractures," J. Pet. Technol., **13**(9), pp. 937–949.
[10] Adachi, J., 2001, "Fluid-Driven Fracture in Permeable Rock," Ph.D. thesis, University of Minnesota, Minneapolis, MN.
[11] Detournay, E., 2004, "Propagation Regimes of Fluid-Driven Fractures in Impermeable Rocks," Int. J. Geomech., **4**(1), pp. 35–45.
[12] Garagash, D. I., 2006, "Propagation of a Plane-Strain Hydraulic Fracture With a Fluid Lag: Early-Time Solution," Int. J. Solids Struct., **43**(18–19), pp. 5811–5835.
[13] Savitski, A. A., and Detournay, E., 2002, "Propagation of a Penny-Shaped Fluid-Driven Fracture in an Impermeable Rock: Asymptotic Solutions," Int. J. Solids Struct., **39**(26), pp. 6311–6337.
[14] Olson, J. E., and Taleghani, A. D., 2009, "Modeling Simultaneous Growth of Multiple Hydraulic Fractures and Their Interaction With Natural Fractures," SPE Hydraulic Fracturing Technology Conference, Society of Petroleum Engineers, The Woodlands, TX, Paper No. SPE-119739-MS.
[15] Taleghani, A. D., 2011, "Modeling Simultaneous Growth of Multi-Branch Hydraulic Fractures," 45th U.S. Rock Mechanics/Geomechanics Symposium, American Rock Mechanics Association, San Francisco, CA, June 26–29, Paper No. ARMA-11-436.
[16] Bunger, A. P., 2013, "Analysis of the Power Input Needed to Propagate Multiple Hydraulic Fractures," Int. J. Solids Struct., **50**(10), pp. 1538–1549.
[17] Bunger, A. P., Jeffrey, R. G., and Zhang, X., 2014, "Constraints on Simultaneous Growth of Hydraulic Fractures From Multiple Perforation Clusters in Horizontal Wells," SPE J., **19**(4), pp. 608–620.
[18] Wu, K., and Olson, J. E., 2015, "Simultaneous Multifracture Treatments: Fully Coupled Fluid Flow and Fracture Mechanics for Horizontal Wells," SPE J., **20**(2), pp. 337–346.
[19] Wu, K., and Olson, J. E., 2015, "Mechanisms of Simultaneous Hydraulic-Fracture Propagation From Multiple Perforation Clusters in Horizontal Wells," SPE J., **21**(3), pp. 1–9.
[20] Zeng, Q., Liu, Z., Wang, T., Gao, Y., and Zhuang, Z., 2017, "Fully Coupled Simulation of the Propagation of Multiple Hydraulic Fractures From a Horizontal Wellbore," Comput. Mech., (submitted).
[21] Zhuang, Z., Liu, Z., Cheng, B., and Liao, J., 2014, *Extended Finite Element Method*, Elsevier & Tsinghua University Press, Oxford, UK.
[22] Fox, R. W., McDonald, A. T., and Pritchard, P. J., 2010, *Introduction to Fluid Mechanics*, Wiley, New York.
[23] Crump, J. B., and Conway, M. W., 1988, "Effects of Perforation-Entry Friction on Bottomhole Treating Analysis," J. Pet. Technol., **40**(8), pp. 1041–1048.
[24] Wang, H., Liu, Z., Xu, D., Zeng, Q., and Zhuang, Z., 2016, "Extended Finite Element Method Analysis for Shielding and Amplification Effect of a Main Crack Interacted With a Group of Nearby Parallel Microcracks," Int. J. Damage Mech., **25**(1), pp. 4–25.
[25] Bažant, Z. P., Ohtsubo, H., and Aoh, K., 1979, "Stability and Post-Critical Growth of a System of Cooling or Shrinkage Cracks," Int. J. Fract., **15**(5), pp. 443–456.
[26] Bažant, Z. P., and Tabbara, M. R., 1992, "Bifurcation and Stability of Structures With Interacting Propagating Cracks," Int. J. Fract., **53**(3), pp. 273–289.
[27] Nemat-Nasser, S., Keer, L. M., and Parihar, K. S., 1978, "Unstable Growth of Thermally Induced Interacting Cracks in Brittle Solids," Int. J. Solids Struct., **14**(6), pp. 409–430.
[28] Nemat-Nasser, S., Sumi, Y., and Keer, L. M., 1980, "Unstable Growth of Tension Cracks in Brittle Solids: Stable and Unstable Bifurcations, Snap-Through, and Imperfection Sensitivity," Int. J. Solids Struct., **16**(11), pp. 1017–1035.